Nanoscale

PAPER

View Article Online
View Journal | View Issue

Cite this: *Nanoscale*, 2025, **17**, 5270

Self-assembly processes of 2D Au(I)–$S(CH_2)_2COOH$ lamellae†

Shengrui Zhang,[a] Zhongqi Yu,[a] Aude Demessence, *[b] Nathalie Guillou,[c] Shujue Xu,[a] Han Liu,[a] Yuru Fu,[a] Jingpei Zhang[a] and Minjie Li *[a]

Received 5th December 2024,
Accepted 17th January 2025

DOI: 10.1039/d4nr05118a

rsc.li/nanoscale

Solving the assembled structure of Au(I)-thiolate linear coordination polymers has been a challenging task as they generally lack good crystallinity. This has prevented the elucidation of their assembly processes at the molecular level. In this paper, selected area electron diffraction (SAED) patterns of two-dimensional (2D) Au(I)–$S(CH_2)_2COOH$ (Au(I)-MPA) lamellae are obtained by applying cryogenic transmission electron microscopy. The SAED patterns allow to propose a packing mode of Au(I)-MPA chains in the 2D structure by comparison with the crystal structure of Ag(I)-MPA solved from powder X-ray diffraction. Then, multi-step self-assembly processes to 2D lamellae *via* the aggregation and crystallization of an intermediate of 1D pre-assemblies are disclosed, which explains the difficulty in synthesize their large single crystals. Based on these results, 2D Au(I)-MPA lamellae with tunable sizes and degrees of crystallinity are synthesized by kinetic control of solvent composition and temperature.

Introduction

Au(I)-thiolate linear coordination polymers are a special type of Au(I)-thiolate complexes (complexes that have Au(I) metal center bonded to thiolate ligands either in the presence or in the absence of other auxiliary ligands[1,2]) that have one dimensional (1D) polymeric structure of $[Au(I)\text{-}SR]_n$.[3,4] To be concise, if we do not mention, Au(I)-thiolate is used to represent Au(I)-thiolate linear coordination polymer for short in this paper. Au(I)-thiolates have been studied for many years because of their important applications as luminescent materials,[5,6] drugs,[7,8] and precursors of gold nanoparticles.[9] In recent years, assemblies of Au(I)-thiolate with different packing structures, morphologies, and dimensional features have been developed. They show properties that make them interesting for a range of emerging applications, including bio-structure mimicking,[10] chiral sensing,[11] temperature detection,[12] phase change materials,[13] and nano-mechanical elements.[14] However, molecular level understanding of the assembly mechanism is still insufficient, especially for those with complex morphological evolution processes. What hinders the mechanistic study is the difficulty of identifying the structure, as most of them do not have sufficient crystallinity to allow single-crystal X-ray diffraction (XRD) characterization,[15] and are also prone to decomposition under the electron beam during high-resolution imaging or electron diffraction measurements.[16,17] Therefore, there is an urgent need to develop methods for revealing the structure of poorly crystallized Au(I)-thiolate assemblies, which will enable to understand the self-assembly mechanisms.

In this aspect, Demessence *et al.* have succeeded in preparing highly crystalline Au(I)-thiolate assemblies (thiolate = 4-mercaptobenzoic acid, methyl 4-mercaptobenzoate, *etc.*) and used high-quality powder X-ray diffraction (PXRD) data to solve their crystal structures.[6] Li and co-workers have shown that solution-phase frequency-modulated atomic force microscopy (AFM) can be directly used to observe the molecular arrangement of surface ligands on highly ordered single-layer Au(I)-thiolate assemblies (thiolate = 3-mercaptopropionic acid (MPA) and glutathione),[14] compensating for the inability of scanning tunneling microscope (STM) to image the thick and insulating assemblies. In addition, different computational calculations have also been used to simulate the structure of Au(I)-thiolate (thiolate = cysteine, Cys),[10] and these advances have made important contributions to the understanding of the structure-property relationship. However, the link between the molecular packing mode and the morphological evolution, which is critical for the assembly processes, is still missing. Since selected area electron diffraction (SAED) is an accurate technique to reveal the molecular packing in morphology-specific crystals, which can make up for the missing link, it is necessary to

[a]*State Key Lab of Supramolecular Structure and Materials, College of Chemistry, Jilin University, Changchun, 130012, P. R. China. E-mail: liminjie@jlu.edu.cn*
[b]*Univ Lyon, Université Claude Bernard Lyon 1, CNRS, Institut de recherches sur la catalyse et l'environnement de Lyon (IRCELYON), Villeurbanne, France. E-mail: aude.demessence@ircelyon.univ-lyon1.fr*
[c]*Université Paris-Saclay, UVSQ, CNRS, UMR 8180, Institut Lavoisier de Versailles, 78000 Versailles, France*

†Electronic supplementary information (ESI) available. CCDC 2385737. For ESI and crystallographic data in CIF or other electronic format see DOI: https://doi.org/10.1039/d4nr05118a

solve the problem of decomposition of Au(I)-thiolates under electron beam during SAED measurement. Cryogenic transmission electron microscopy (Cryo-TEM) has been explored to solve the problem of sample instability for different types of materials, especially biological[18] and highly sensitive samples,[19] therefore, it is worthwhile to use Cryo-TEM for SAED measurement of Au(I)-thiolate crystals.

Here, the two-dimensional (2D) Au(I)–S$(CH_2)_2$COOH (Au(I)-MPA) lamellae, with multiple structural transformation steps but no confirmed assembly processes at molecular level, is chosen as the material of study.[11,17,20–24] To avoid the fast decomposition of the sample under electron beam, Cryo-TEM with low dose electron beam and short electron beam exposure time is applied. This, combined with the increased sample size and crystallinity, allows to obtain SAED patterns. With them and a reference structure of 2D Ag(I)-MPA crystals, a packing mode of Au(I)-MPA chains in the 2D structure *via* short inter-chain aurophilic interactions (Au(I)–Au(I) distance = 2.84 Å) in intra-layers, and strong inter-ligand H-bonds in inter-layers is proposed. Then multiple-step assembly processes are disclosed, which involve the fast formation and growth of one-dimensional (1D) pre-assemblies and the subsequent aggregation and crystallization of these 1D pre-assemblies to 2D lamellae. And the growth of 1D pre-assemblies is found to compete with their aggregation and crystallization to 2D lamellae, the larger the 1D pre-assemblies, the more difficult their transformation to 2D lamellae. The complicated assembly processes explain why it is difficult to obtain highly crystalline single-crystals, and also indicate the importance of kinetic control to improve their crystallinity. Finally, an effective method to tune the size and degree of the crystallinity of 2D Au(I)-MPA lamellae is demonstrated by controlling the assembly processes with both solvent composition and temperature, which is very important for studying their physical properties, such as nonlinear optics and 2D charge carrier transportation.

Experimental section

Materials

All chemicals are commercially available and used without further purification. Hydrogen tetrachloroaurate(III) hydrate ($HAuCl_4{\cdot}4H_2O$, AR grade) and silver nitrate ($AgNO_3$, AR grade) were purchased from Sinopharm Chemical Reagent Co., Ltd. 3-Mercaptopropionic acid (MPA, ≥99%) was purchased from Alfa Aesar Company. Sodium hydroxide (NaOH, ≥96%) and ethylene glycol (EG, ≥99%) were purchased from Beijing Chemical Industry Reagent Company. Sodium 3-mercaptopropionate (MPA-Na) was obtained by 1 : 1 molar ratio neutralization of MPA with NaOH. Water was purified by the Milli-Q system.

Characterizations

UV-vis absorption spectra were measured using an Analytik Jena Specord®210 plus UV/VIS spectrophotometer (wavelength resolution: 0.1 nm) with 1 cm light path cuvettes. The scan step was set as 1 nm. Transmission Electron Microscope (TEM) images were obtained using a JEM-2100F electron microscope operating at 200 kV. Samples were deposited onto carbon-coated copper grids for the measurements. Atomic force microscopy (AFM) images (samples in dry state) were recorded with tapping mode with a Nanoscope IIIa scanning probe microscope from Digital Instruments under ambient conditions, and samples were adsorbed on (3-aminopropyl) triethoxysilane-modified mica plates for AFM characterization. Powder X-ray diffraction (PXRD) data were collected with an Empyrean diffractometer with Cu Kα radiation (λ = 1.5418 Å). Tube voltage and current were 40 kV and 40 mA, respectively; scan range (2θ) was from 5.0° to 60.0°, and scan speed was 0.1° min^{-1}. Optical microscopic images were obtained using a Leica DM4000 M LED Optical Microscope. Samples were deposited onto microscope slide for their measurements. The cryogenic transmission electron microscopy (Cryo-TEM) experiments were performed with a thin film of sample solution (3 μL) transferred to a lacey carbon supported copper grid. The excess liquid was blotted with filter paper for 2–3 seconds, and the thin films were rapidly vitrified by plunging them into liquid ethane (cooled by liquid nitrogen) at its freezing point. The grid was transferred on a Gatan 626 cryoholder, using a cryo-transfer device and transferred to the FEI Talos F200C TEM. Direct imaging was carried out at a temperature of approximately −175 °C and with a 200 kV accelerating voltage, using the images acquired with a Dual vision 300 W and SC 1000 CCD camera (Gatan, Inc.; Warrendale, PA). Synchrotron radiation PXRD was measured at BL14B1 beamline at shanghai synchrotron radiation facility (λ = 0.6887 Å). All calculations of structural investigation were performed with the TOPAS program (indexing, simulated annealing, Rietveld refinement).[25] The LSI-indexing method converged to a monoclinic unit cell with satisfactory figure of Merit (see Table S1†). Systematic extinctions were consistent with the $P2_1/c$ space group, which was used to initialize the structural determination. The structure was solved in the direct space by using the simulated annealing process. The MPA ligand was treated as rigid body by allowing the free rotation of the carboxylate function. The MPA molecule was allowed to move around the sulfur atom together with the Ag(I) and a soft restrain of 2.3 Å on the Ag(I)–S distance was applied. The final Rietveld plot (Fig. S6†) corresponds to satisfactory model indicator and profile factors (see Table S1†). This involved the following structural parameters: 1 scale factor, 3 atomic coordinates for Ag(I), 6 parameters for the orientation and the translation of the MPA ligand, 5 distances and 6 angles inside the organic molecule and 3 temperature factors. The crystal structure quoted the depository number CCDC- 2385737. X-ray photoelectron spectroscopy (XPS) measurements were carried out at 15 kV and 17 mA, using a Thermo ESCALAB 250 spectrometer with a twin-anode Al Kα (1486.6 eV) X-ray source.

Preparation

All glass flasks and burets were cleaned thoroughly with aqua regia before use.

Preparation of 2D Au(I)-MPA-EG lamellae at 100, 110 and 126 °C (water content = 10%) and monitoring of assembly processes. A mixture of 0.800 mL MPA-Na (5.00×10^{-2} M) and 0.200 mL NaOH (1.00×10^{-1} M) aqueous solution were added to 10 mL EG in an Erlenmeyer flask at room temperature, and then 0.200 mL $HAuCl_4$ (5.00×10^{-2} M) aqueous solution was added under stirring. The solutions were heated to 100, 110 °C and boiling temperature (126 °C), then samples were taken out at different time intervals for TEM and (or) spectral measurements to monitor the assembly processes and determine the completion time of self-assembly. According to the results, the same reactions were allowed to take place at 100, 110 and 126 °C for 20, 15 and 15 min, respectively, to obtain the final products, which are denoted as Au(I)-MPA-EG-X (X = 100, 110 and 126 °C).

Preparation of 2D Ag(I)-MPA lamellae. 0.200 mL MPA-Na (5.00×10^{-2} M) aqueous solution was injected to 10 mL $AgNO_3$ aqueous solution (1.00×10^{-3} M) in an Erlenmeyer flask at room temperature. Then the solution was boiled for 30 min and cooled to room temperature naturally to obtain the colloidal solution of 2D Ag(I)-MPA lamellae.

Preparation of 2D Au(I)-MPA-EG lamellae at 100 and 176 °C (water content = 1.78%). A mixture of 0.800 mL MPA-Na (5.00×10^{-2} M) and 0.200 mL NaOH (1.00×10^{-1} M) EG solution was added to 10 mL EG in an Erlenmeyer flask at room temperature, and then 0.200 mL $HAuCl_4$ (5.00×10^{-2} M) aqueous solution was added under stirring. The solutions were heated to 100 °C or boiling temperature (176 °C) for 1 h, then cooled to room temperature naturally to obtain the colloidal solution of 2D Au(I)-MPA-EG lamellae.

Preparation of 2D Au(I)-MPA lamellae in water/EG mixture (water content = 10%–50%). A mixture of 0.080 mL MPA-Na (5.00×10^{-1} M) and 0.020 mL NaOH (1.00 M) aqueous solution was injected to (10-*a*) mL EG in an Erlenmeyer flask at room temperature (*a* = 5.0, 4.0, 3.0, 2.0 and 1.0 mL), and then 0.020 mL $HAuCl_4$ (5.00×10^{-1} M) aqueous solution was added under stirring. Then the solutions were heated in an oil bath (130 °C) for 10 min, *a* mL water was added and then the reaction continued for 15 min to obtain the 2D lamellae. The obtained colloidal products are denoted as 2D Au(I)-MPA lamellae-*Y* (*Y* = water content = 50, 40, 30, 20, and 10% respectively), and the water content ranged from 10% to 50%. Note: EG is reductive, and Au^{3+} is reduced to Au nanoparticles when $HAuCl_4$ is added to EG without MPA. Therefore, $HAuCl_4$ aqueous solution is added to the EG solution containing MPA to avoid their reduction to gold nanoparticles.

Purification of 2D Au(I)-MPA and Ag(I)-MPA lamellae

2D Au(I)-MPA and Ag(I)-MPA lamellae were separated from the solution with a centrifuge to remove the soluble un-assembled species, the separated lamellae were washed with water for two times to get the purified lamellae.

Measurement of the yields

The theoretical weight of the 2D lamellae was calculated assuming all the Au ions have been transformed into 2D Au(I)-MPA lamellae with Au and thiolate ligand in 1 : 1 molar ratio. 2D Au(I)-MPA lamellae were separated from the solution with a centrifuge to remove the soluble un-assembled species, the dried samples were weighted to get the experimental weights. The yield of the 2D lamellae was calculated to be 73, 76, 80, 84 and 88% at water content of 10, 20, 30, 40 and 50%, respectively.

Results and discussion

Design

Au(I)-thiolate linear coordination polymers are a class of self-assembled crystalline materials that can exhibit extremely complex structural evolution processes because of the 1D polymeric structure.[10,15,20] For example, when chiral ligand with multiple functional groups, such as Cys, is used, they can form structures of high complexity,[10] which poses a great challenge to understanding the assembly mechanism. Even achiral ligands with relatively simple inter-ligand interactions, such as MPA, is used, they also undergo multi-step morphology transformation processes from 1D pre-assemblies to 2D lamellae as we have disclosed earlier.[20] The morphological evolution processes of Au(I)-MPA have a moderate complexity and are different from those exhibited by other coordination polymers,[26] therefore, it was selected as a model system to reveal its packing structure and then correlate the structures to the assembly processes.

As we have mentioned above, it is difficult to directly characterize the packing mode of Au(I)-thiolate chains inside the assemblies by applying common diffraction methods[6,27] and microscopic imaging methods[14,28] because of the decomposition of Au(I)-thiolate assemblies under electron beam. Our previous work shows that the edges of 2D Au(I)-MPA lamellae or thin samples can more easily turn into gold nanoparticles under electron beam than the center or thick samples (Fig. S1†). Therefore, if the size and crystallinity of the products can be improved on the one hand, and if less destructive TEM conditions (such as short electron exposure time, low dose of electron beam and low temperature, which are available in Cryo-TEM) are applied on the other hand, it is possible to obtain their high-resolution images or SAED before their decomposition.

Synthesis of large-sized 2D Au(I)-MPA lamellae with improved crystallinity and the structural resolution

In our previous work, we found that changing solvent from water to ethylene glycol (EG) (containing about 10% water, which is brought by the aqueous solution of the reactants) can afford 2D Au(I)-MPA lamellae with significantly increased sizes and improved crystallinity, but their packing structure is different from those prepared in water.[24] Here, by lowering the synthetic pH value from *ca.* 6.5 in the previous work to *ca.* 5.0 in this work, the samples prepared in the two solvents (denoted as Au(I)-MPA-water and EG, respectively) have the same molecular packing as estimated from the same UV-vis

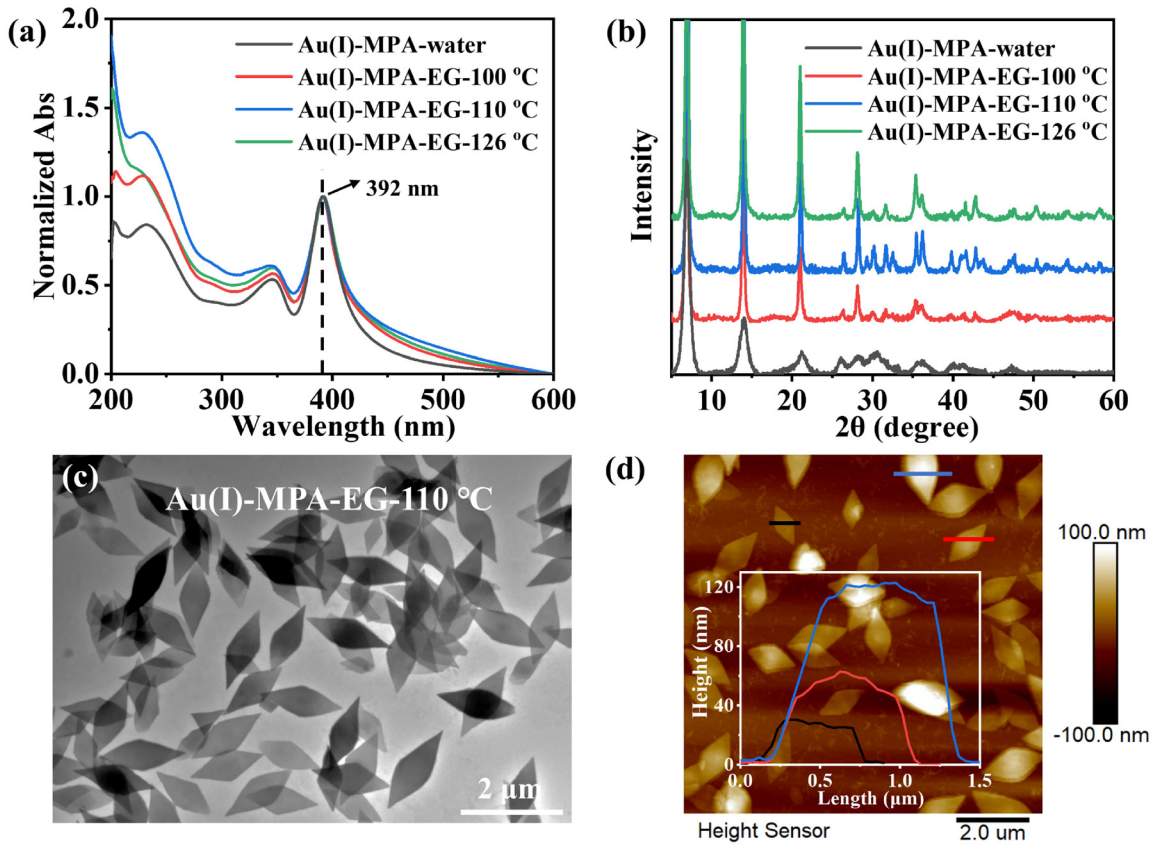

Fig. 1 UV-vis spectra (a) and PXRD patterns (b) of Au(I)-MPA-water and Au(I)-MPA-EG-100/110/126 °C ([Au] = 1.00 × 10^{-4} M in UV-vis spectra); (c) TEM and (d) AFM images of Au(I)-MPA-EG-110 °C and their height analyses.

absorption peak (Fig. 1a) and inter-layer PXRD peaks (Fig. 1b),[24,29,30] and Au(I)-MPA-EG samples, regardless of the synthetic temperatures, *i.e.* 100, 110 and 126 °C (boiling temperature of the solvent, EG with 10% water in volume) all show much improved PXRD patterns as compared with Au(I)-MPA water (synthesized at boiling temperature of water, *ca.* 100 °C). Surprisingly, the crystallinity of sample Au(I)-MPA-EG first increases and then decreases as the temperature lowers from 126 °C to 110 °C and then to 100 °C as indicated from their PXRD peak numbers (Fig. 1b and Fig. S2†). The reasons will be discussed after the molecular-level assembly processes are revealed in the later section. Thus, sample of Au(I)-MPA-EG-110 °C is selected for SAED and PXRD measurements. In addition, the much larger size of the highly crystalline Au(I)-MPA-EG-110 °C (rhombus lamellae, long diagonal of 1–2 μm, thickness of 25–120 nm, Fig. 1c and d) than Au(I)-MPA-water (irregular lamellae, sub micrometer in size and less than 15 nm in thickness)[23] is advantageous to increasing the electron endurance.

We first attempt to use ordinary TEM to image Au(I)-MPA-EG-110 °C, and find this sample is more stable as compared to the smaller Au(I)-MPA-water sample, but they still decompose into gold nanoparticles under the focused electron beam during SAED measurement (Fig. S3†). When Cryo-TEM is employed, SAED patterns of sample Au(I)-MPA-EG-110 °C can be obtained before its decomposition at low electron beam dose (<10 pA cm^{-2}) and short electron beam exposure time (<2 s) (Fig. 2a and b), while sample Au(I)-MPA-water is quickly destroyed in the same condition (Fig. S4†). SAED of Au(I)-MPA-EG-110 °C shows clear rectangular pattern of diffraction points, which indicates that they are single crystals. The two nearest pairs of diffraction points (*C*, *C*′ and *D*, *D*′) are along the direction of the two diagonals of the rhombus 2D lamella (OA and OB), respectively, which are calculated to be 2.84 and 3.19 Å by averaging ten sets of data. Because it is unable to tilt the sample holder in the Cryo-TEM, 3D SAED patterns cannot be obtained so far. Nevertheless, the fact that the 2D layers stack parallel to the surfaces of TEM substrate of copper grid[20] allows us to directly relate the 2.84 and 3.19 Å to two in-plane *d*-spacings without inter-layer contribution. These two in-plane *d*-spacings correspond to diffraction peaks at 31.50° and 27.96°, which are very close to the two PXRD peaks at 31.60° (2.83 Å) and 28.05° (3.16 Å) (Fig. S5†). It is ideal we extract the lattice parameters from PXRD, however, the broad diffraction peaks did not allow us to do it unambiguously.

In order to assign the *d*-spacings obtained from SAED and infer the arrangement of Au(I)-MPA chains in the rhombus 2D lamellae, a reference sample of Ag(I)-MPA lamellae, which has much better crystallinity than Au(I)-MPA lamellae, is prepared and its structure is solved *ab initio* from synchrotron

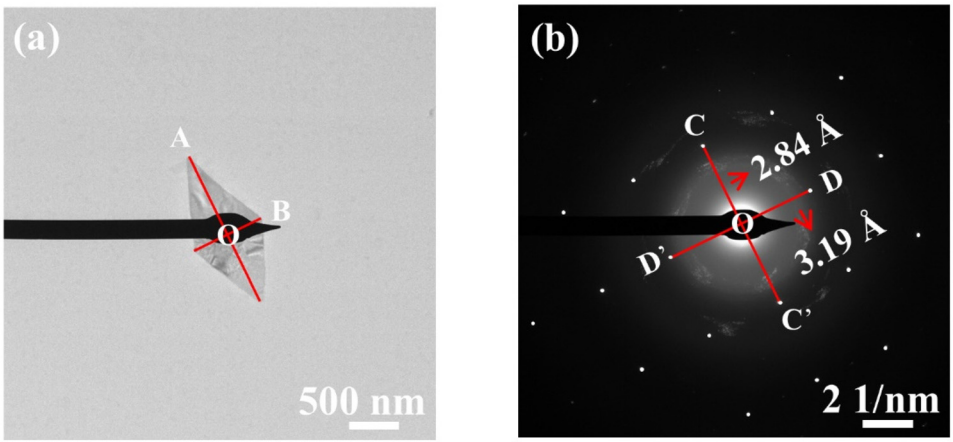

Fig. 2 Cryo-TEM image (a) and SAED pattern (b) of Au(I)-MPA-EG-110 °C. White dots have been added to highlight the diffraction spots.

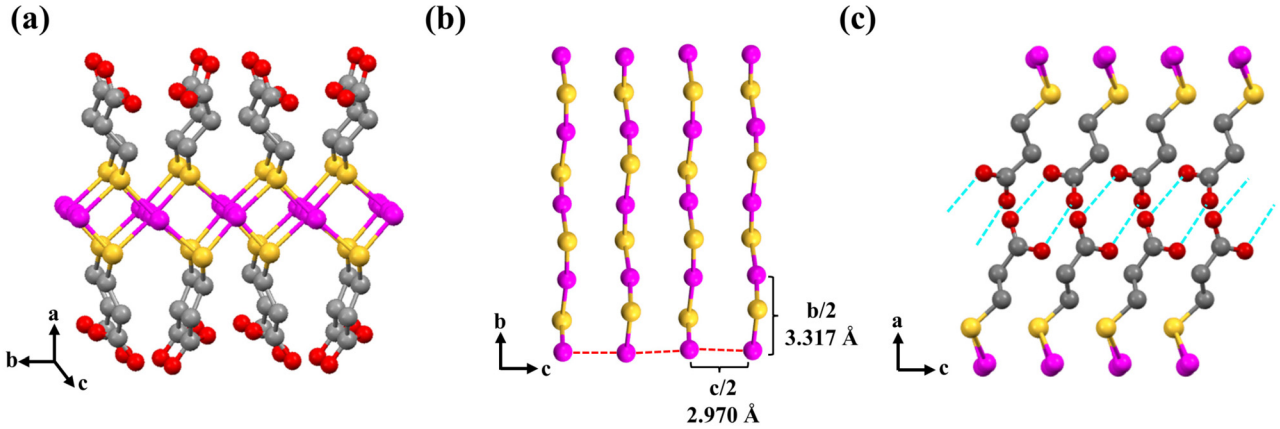

Fig. 3 (a) Packing of Ag(I)-MPA chains in the 2D lamellae; (b) view of Ag(I)-MPA chains bond through the argenphilic interactions (red dashed lines); (c) illustration of the inter-ligand H-bonds (blue dashed lines). Pink, yellow, grey and red spheres represent Ag, S, C and O atoms, respectively. Hydrogen atoms have been omitted for clarity.

irradiation PXRD. Ag(I)-MPA crystallizes in the monoclinic $P2_1/c$ space group, with the following lattice parameters: a = 13.6120(2) Å, b = 6.633726(6) Å, c = 5.94002(5) Å, β = 99.695(1)° (Fig. S6 and Table S1†). In the structure, zig-zag –S–Ag(I)–S– chains have a staggered side-by-side packing to form a layered structure. The intra-chain Ag–Ag distance is $b/2$ = 3.317 Å, and inter-chain Ag–Ag distance is $c/2$ = 2.970 Å (Fig. 3b). The layers are then connected through inter-ligand H-bonds with inter-layer distance of 13.42 Å (13.61 Å·sin 99.695°) (Fig. 3c). This type of structure of Ag(I)-MPA has not been reported in other Ag(I)-thiolate crystals as far as we know,[3,31] but it is similar to some 2D Au(I)-thiolate crystals, such as $[Au(p\text{-}SPhCO_2Me)]_n$ and $[Au(SEtPh)]_n$ that have comparable in-plane lattice parameters.[6,13] Based on the fact that Au(I)-MPA and Ag(I)-MPA can co-assemble,[32] we suggest that Au(I)-MPA chains also have similar staggered side-by-side packing, therefore, the d-spacings of 2.84 Å and 3.19 Å are suggested as the inter-chain and intra-chain Au-Au distances, indicative of strong inter-chain aurophilic interactions and the presence of intra-chain aurophilic interactions.[3] By comparing the morphology of the lamellae with the SAED pattern, it is proposed that –S–Au(I)–S– chains align along the short diagonal (OB) of the rhombic 2D lamellae (Fig. 2a).

Self-assembly processes of 2D Au(I)-MPA lamellae

After the chain arrangement in 2D Au(I)-MPA lamellae is proposed, molecular level assembly processes is further revealed, with samples of Au(I)-MPA-EG-110 °C and Au(I)-MPA-EG-126 °C as examples, to understand why the crystallinity of sample prepared at a higher temperature of 126 °C is lower than that prepared at 110 °C (Fig. 4 and Fig. S7, S8†). Au(I)-MPA-EG prepared at both 110 °C and 126 °C have similar assembly processes as that occurs in water, which all involve the formation of 1D pre-assemblies.[23] However, in the case of sample Au(I)-MPA-EG-126 °C, the transformation processes from 1D pre-assemblies into 2D lamellae are clearer (Fig. 4b–h and Fig. S7†). The TEM images show that soft 1D pre-assemblies are generated first (Fig. 4b) with the absorption at <370 nm at

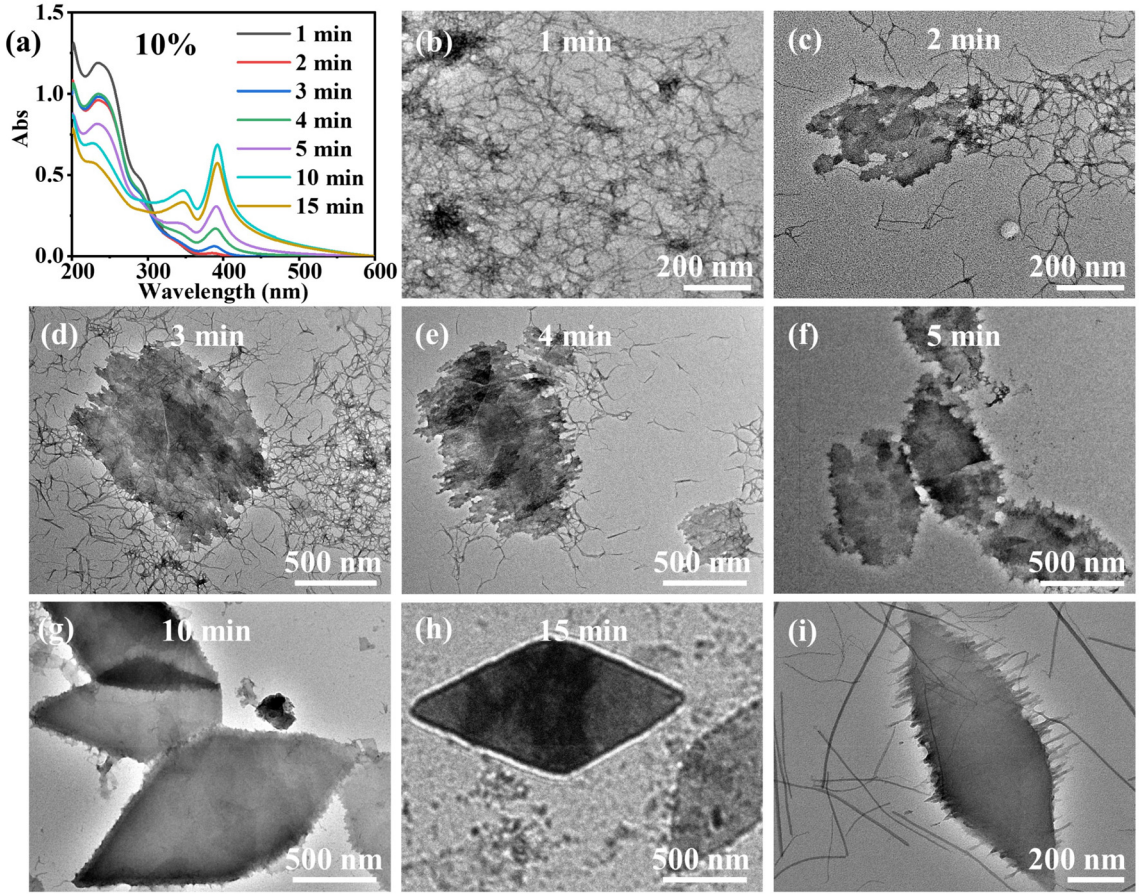

Fig. 4 UV-vis spectra (a) and typical TEM images (b–h) of Au(I)-MPA-EG-126 °C samples at different time ([Au] = 1.00 × 10^{-4} M in UV-vis spectra); (i) a specific TEM image of the intermediate products showing the relationship between 1D pre-assemblies and 2D lamellae at about 5–10 min.

1 min (Fig. 4a). At 2 min, irregularly shaped 2D lamellae are present in addition to 1D pre-assemblies (Fig. 4c), which corresponds to the appearance of a tiny absorption at ~386 nm typical for small and less-regular 2D lamellae. At 3 and 4 min, larger 2D lamellae with irregular shapes and very rough edges are formed by attachment of smaller ones (Fig. 4d and e) and the absorption of 2D lamellae increases and shifts to ~388 nm. At 5 and 10 min, the 2D lamellae take on a near-rhombic shape with rough edges (Fig. 4f and g) and the absorption further increases and shifts to 392 nm. During this time, 1D pre-assemblies are observed protruding on the edges of the quasi-rhombic 2D lamellae along the direction of the short diagonal in some samples (Fig. 4i), suggesting the rhombic 2D lamellae are formed by side-by-side packing of 1D pre-assemblies. At 15 min, the rough edges of the 2D lamellae become smooth (Fig. 4h), and the absorption at ~392 nm decreases slightly due to the precipitation of the products. The gradual red-shift of the absorption for 2D lamellae from 386 to 392 nm is a result of the increased crystallinity of the assemblies with time.[20]

Besides transforming to 2D lamellae, 1D pre-assemblies are also observed to grow with time, which then in turn slows down their transformation rate to 2D lamellae. The 1D pre-assemblies are soft and thin (2–3 nm in width) (Fig. 4b) at the beginning of formation, and it is easier for them to complete the structural transformation to 2D lamellae, so they are not observed on the irregular edges of 2D lamellae in the TEM images (Fig. 4c–e). As the assembly time proceeds, 1D pre-assemblies grow stiffer and thicker (3–12 nm in width, Fig. 4i), and it is more difficult for them to rapidly transform into 2D lamellae because the structural transformation must undergo the breaking and reforming of the inter-molecular interactions, therefore, the intermediate state of 1D pre-assemblies protruding on the edges of 2D lamellae is observed. While in terms of sample Au(I)-MPA-EG-110 °C, the 1D pre-assemblies are soft from the beginning to the end (Fig. S8†), and it is easier for them to crystallize to 2D lamellae. Therefore, Au(I)-MPA-EG-110 °C takes on a near-rhombic shape without the appearance of irregular-shaped intermediates from the beginning of formation to the end. Thus, the final products have a better PXRD pattern as compared to the samples prepared at 126 °C. However, the crystallinity of Au(I)-MPA-EG-100 °C decreases significantly compared to Au(I)-MPA-EG-110 °C (Fig. S2†), indicating that crystallization requires a sufficiently high temperature. From the above results, we can conclude the involvement of 1D pre-assemblies in the crystallization pro-

cesses and the competing growth of 1D pre-assemblies with time (which increase the difficulty for their further structural transformation to 2D lamellae) make Au(I)-MPA difficult to grow into large single crystals, and the crystallinity of the products will not simply increase with the synthetic temperature because of the demonstrated complex structural transformation processes. However, no similar 1D pre-assemblies are found in Ag(I)-MPA,[32] we suggest it is because argenphilic interactions are weaker than aurophilic interactions, and 1D pre-assemblies are not stable for Ag(I)-MPA. Structural adjustment is also easier when intermolecular interactions are weak, so Ag(I)-MPA can grow into crystals with much better crystallinity than Au(I)-MPA.

The observation of the incomplete transformation of 1D pre-assemblies on the edges of 2D lamellae in sample Au(I)-MPA-EG-126 °C also helps us deduce the structure of 1D pre-assemblies. Since 1D pre-assemblies can merge with the 2D lamellae on the edges, they should have similar packing structures, that is, the 1D pre-assemblies are also formed by inter-chain and intra-chain aurophilic interactions in in-plane structure, and H-bonds between ligands of nearby layers. Because the chains are suggested to pack along the short diagonal direction (OB), and the 1D pre-assemblies are also along this direction, the Au(I)-MPA chains are estimated to pack along the 1D direction of pre-assemblies (Fig. 5). The difference in absorption spectra between 1D pre-assemblies (at <370 nm, black line in Fig. 4a) and 2D lamellae (sharp peak at 392 nm, yellowish-brown line in Fig. 4a) indicates that there are still some differences in the packing details, such as structural regularity, packing parameters and (or) ligand conformations. These similarities and differences can also be inferred from the same position but broader width of binding energy of Au and S elements of 1D pre-assemblies than the 2D lamellae in XPS (Fig. S9 and Table S2†).

To sum up, the assembly processes involve (i) fast formation of metastable 1D pre-assemblies *via* inter-chain aurophilic interactions and inter-ligand H-bonds upon mixing the reactants, (ii) aggregation and crystallization of 1D pre-assemblies to form irregular-shaped 2D lamellae by breaking and reforming the interactions, and (iii) reshaping of irregular-shaped 2D lamellae to rhombic 2D lamellae to minimize the surface energies (Fig. 5). The re-shaping process from irregular-shaped 2D lamellae to the final rhombic 2D lamellae is more likely to occur *via* chain sliding on the crystal fronts as that happens in polymer crystallization,[33] rather than *via* the desorption and re-adsorption of Au(I)-MPA chains, because the 2D lamellae do not disassemble at much higher temperature than the crystallization temperature, 176 °C for example as we describe in the next section.

So far, no clear conclusion can be provided to explain why the irregular structure transforms into specific rhombus-shaped 2D lamellae. Since no similar shape in the initial growth is observed (Fig. 4b and c), it can be assumed that the final shape is mainly determined by thermodynamic factors. In addition, when the assembly takes place at a higher pH value (6.84), the assembly tends to form lamellae with a rectangular shape (Fig. S10†). Since pH mainly affects the interactions between ligands, it can be suggested that the shape results from thermodynamic factors that are related to inter-ligand interactions.

Control of the size and crystallinity of 2D Au(I)-MPA lamellae with solvent composition and temperature

Optical and electronic properties, such as non-linear optics,[34] charge carrier transportation[35] of covalent 2D materials have attracted intensive investigation in recent decades, however, most of the physical properties on 2D Au(I)-thiolate coordination polymers are concentrated on their photoemission[13] and electron conduction properties,[36] this is mainly because of their uncontrollable small size and less perfect crystallinity, so we try to explore efficient methods to control the size and crystallinity of Au(I)-MPA lamellae in this section.

The above complicated assembly processes indicate tuning the size and crystallinity cannot be simply achieved by tuning a single experimental parameter, for example, temperature. Here we demonstrate that tuning both solvent composition

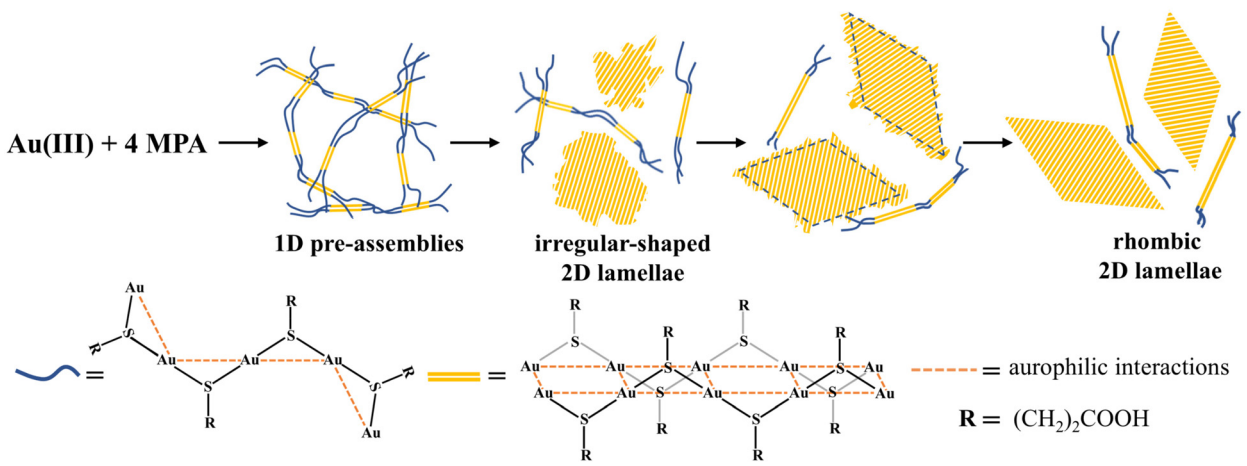

Fig. 5 Schematic illustration of the assembly processes of 2D Au(I)-MPA lamellae starting from Au(III) and MPA *via* 1D pre-assemblies.

and temperature can efficiently control the size and crystallinity of Au(I)-MPA lamellae.

The synthetic solvents we choose are still water and EG because of the good solubility of the reactants and their miscibility. First, the results of the assembly of Au(I)-MPA in water and EG at the same temperature (*ca.* 100 °C) and same concentration ([Au] = 1.00×10^{-3} M) are compared. The assembly of Au(I)-MPA in water is fast and small sub-micrometer 2D lamella are generated within 3 min with a yield of >90%, and their crystallinity is not good.[22] When the assembly happens in nearly pure EG (containing 1.78% of water, introduced with $HAuCl_4$ aqueous solution), a large amount of remaining 1D pre-assemblies are present together with the very large 2D lamellae after 60 min of reaction as indicated by the much stronger absorption at <370 nm typical for 1D pre-assemblies than the absorption for 2D lamellae at 392 nm (Fig. S11a†) and co-existence of aggregates of 1D pre-assemblies with micrometer sized crystals in the optical image (Fig. S11b†). The above control experiments indicate water has a lower solubility of Au(I)-MPA 1D pre-assemblies than EG, and it can speed up the structural transformation of 1D pre-assemblies into 2D lamellae, most probably because of the existence of additional hydrophobic interactions in water. The low solubility of Au(I)-MPA 1D pre-assemblies in water leads to more aggregates of them, therefore, the size of the generated 2D lamellae is small, in the meanwhile, the fast structural transformation rate from 1D pre-assemblies to 2D lamellae, besides the relatively low assembly temperature, are suggested as the reasons for their poor crystallinity. The solubility of Au(I)-MPA 1D pre-assemblies also highly depends on temperature. For example, only 1D pre-assemblies are observed at [Au] = 1.00×10^{-3} M at 176 °C in EG (containing 1.78% of water) (Fig. S12†), and until [Au] is three to four times higher, large 2D lamellae (>4 μm) are generated (Fig. S13†). Therefore, if the assembly occurs in a series of mixture solvents of water and EG at their boiling temperatures, the assembly processes can be significantly tuned.

In order to keep the same 1D pre-assemblies, they are firstly produced in EG by adding the whole aqueous solution of MPA-Na, $HAuCl_4$ and NaOH into it, and allowing it to react and assemble at 130 °C for 10 min, then different amounts of water is added to adjust the solvent composition (water content = 10%–50%). The solution is then heated to boiling for further assembly and crystallization (experimental part 4). Water content above 50% was not tested because the boiling temperature is close to that of water. The samples prepared in mixture solvents are all significantly larger than that synthesized in water, which can be observed with optical microscopy (Fig. S14†), and the size can be tuned in micrometer range, and the higher the water content, the smaller the product size (Fig. 6). The 2D lamellae are of near-rhombic shape with relatively clear edges at water content of 50 and 40%, and of olive-like shape at water content from 30 down to 10% (Fig. 6a–f).

The characteristic UV-vis absorption peaks (392 nm) and typical XRD peaks of the 2D lamellae synthesized in mixture solvents are almost at the same positions (Fig. S15 and S16†). However, smaller 2D lamellae with lower assembly temperature at higher water contents have better crystallinity, which appears to be related to the complex assembly processes and the competition between the growth of 1D pre-assemblies and the crystallization of 2D lamellae. It is worth mentioning that the sample with 50% of water content exhibits three tiny additional peaks at 27.17, 33.80 and 38.64° that do not appear

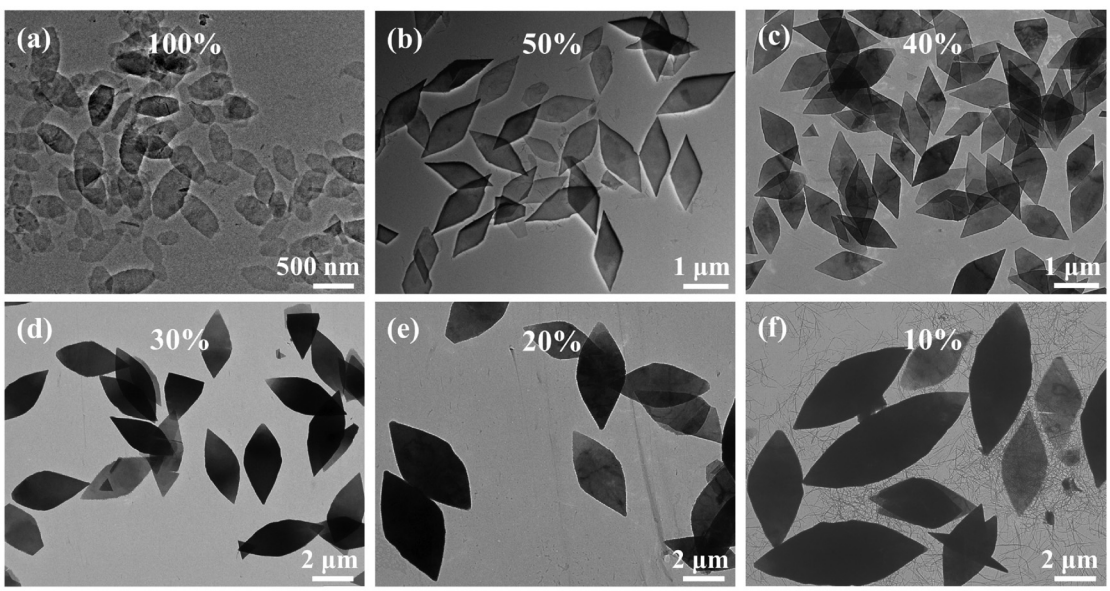

Fig. 6 TEM images of 2D Au(I)-MPA lamellae prepared with different water contents. (a) 100%, (b) 50%, (c) 40%, (d) 30%, (e) 20%, (f) 10%.

in all other PXRD, indicating that some minor impurities are likely to have generated in this condition (Fig. S16 and S17†), which adds complexity to the assembly processes. Nevertheless, the results show that tuning the solvent composition and temperature is a convenient method to achieve kinetic control of the size and crystallinity of the 2D lamellae, and it avoids the use of other techniques such as hydrothermal or solvothermal synthesis to improve the crystallinity by increasing the temperature.[6,12] This method can in principle be extended to the synthesis of other Au(I)-thiolate crystals.

Conclusions

To overcome the problem in stability of Au(I)-thiolate assemblies under electron beam, larger 2D Au(I)-MPA lamellae with relatively good crystallinity were synthesized, for which Cryo-TEM with low electron beam dose and short exposure time to get the SAED patterns was applied. Referring to SAED and a similar reference structure of 2D Ag(I)-MPA crystals, a packing mode of Au(I)-MPA chains in the 2D structure was proposed. Then multi-step self-assembly processes involving the 1D pre-assemblies and their aggregation and crystallization to 2D lamellae are disclosed. The existence of 1D pre-assemblies with strong inter-chain interactions and H-bonds, as well as the requirement to break and reform bonds are proposed as the main reasons why Au(I)-MPA, and probably other similar Au(I)-thiolates, are difficult to grow into large single crystals. Finally, a practical strategy to tune the size and crystallinity of such a 2D lamella *via* changing the solvent composition and temperature is demonstrated. This approach that allows to obtain a 2D Au(I)-MPA lamella with tunable micrometer sizes and different degrees of crystallinity. Since Au(I)-MPA-EG lamellae have higher structural anisotropy than the conventional covalent 2D materials, they may show higher non-linear optical effects and anisotropic charge carrier transportation behaviors. When the size of the high crystalline Au(I)-MPA-EG reaches micrometers, it is possible to study these properties, and we will continue to work on it.

Author contributions

M. Li conceived the project. S. Zhang and Z. Yu synthesized Au(I)-MPA and Ag(I)-MPA samples and did most of the characterizations. S. Xu, Y. Fu, J, Zhang, and H. Liu did some supplementary synthesis and characterizations. N. Guillou and A. Demessence solved the structure of Ag-MPA from the synchrotron PXRD, S. Zhang, N. Guillou, A. Demessence and M. Li discussed the results and co-wrote the final paper.

Data availability

The authors confirm that the data supporting the findings of this study are available within the article and its ESI.†

Conflicts of interest

The authors declare no conflict of interest.

Acknowledgements

This work is supported by NSFC (21574058).

References

1 H. Schmidbaur and A. Schiera, Aurophilic interactions as a subject of current research: an up-date, *Chem. Soc. Rev.*, 2012, **41**, 370–412.
2 T. Zou, C. T. Lum, C.-N. Lok, J.-J. Zhang and C.-M. Che, Chemical biology of anticancer gold(III) and gold(I) complexes, *Chem. Soc. Rev.*, 2015, **44**, 8786–8801.
3 O. Veselska and A. Demessence, d^{10} coinage metal organic chalcogenolates: From oligomers to coordination polymers, *Coord. Chem. Rev.*, 2018, **355**, 240–270.
4 M. Murakami, R. Matsumine, T. Ono and K. Konishi, Self-assembling-directed Growth and PL Evolution of a Soluble Gold Thiolate Coordination Polymer, *Chem. Lett.*, 2020, **49**, 1228–1231.
5 S.-H. Cha, J.-U. Kim, K.-H. Kim and J.-C. Lee, Preparation and Photoluminescent Properties of Gold(I)-Alkanethiolate Complexes Having Highly Ordered Supramolecular Structures, *Chem. Mater.*, 2007, **19**, 6297–6303.
6 C. Lavenn, N. Guillou, M. Monge, D. Podbevsek, G. Ledoux, A. Fateeva and A. Demessence, Shedding light on an ultra-bright photoluminescent lamellar gold thiolate coordination polymer $[Au(p\text{-}SPhCO_2Me)]_n$, *Chem. Commun.*, 2016, **52**, 9063–9066.
7 C. F. Shaw, Gold-based therapeutic agents, *Chem. Rev.*, 1999, **99**, 2589–2600.
8 C.-M. Che and R. W.-Y. Sun, Therapeutic applications of gold complexes: lipophilic gold(III) cations and gold(I) complexes for anti-cancer treatment, *Chem. Commun.*, 2011, **47**, 9554–9560.
9 Y. Negishi, K. Nobusada and T. Tsukuda, Glutathione-protected gold clusters revisited: bridging the gap between gold(I)-thiolate complexes and thiolate-protected gold nanocrystals, *J. Am. Chem. Soc.*, 2005, **127**, 5261–5270.
10 W. Jiang, Z.-B. Qu, P. Kumar, D. Vecchio, Y. Wang, Y. Ma, J. H. Bahng, K. Bernardino, W. R. Gomes, F. M. Colombari, A. Lozada-Blanco, M. Veksler, E. Marino, A. Simon, C. Murray, S. R. Muniz, A. F. de Moura and N. A. Kotov, Emergence of complexity in hierarchically organized chiral particles, *Science*, 2020, **368**, 642–648.
11 Y. Yu, G. Yang, S. Zhang, M. Liu, S. Xu, C. Wang, M. Li and S. X.-A. Zhang, Wide-Range and Highly Sensitive Chiral Sensing by Discrete 2D Chirality Transfer on Confined Surfaces of Au(I)-Thiolate Nanosheets, *ACS Nano*, 2022, **16**, 148–159.

12 O. Veselska, L. Okhrimenko, N. Guillou, D. Podbevsek, G. Ledoux, C. Dujardin, M. Monge, D. M. Chevrier, R. Yang, P. Zhang, A. Fateeva and A. Demessence, An intrinsic dual-emitting gold thiolate coordination polymer, $[Au(+I)(p\text{-}SPhCO_2H)]_n$, for ratiometric temperature sensing, *J. Mater. Chem. C*, 2017, **5**, 9843–9848.

13 O. Veselska, S. Vaidya, C. Das, N. Guillou, P. Bordet, A. Fateeva, F. Toche, R. Chiriac, G. Ledoux, S. Wuttke, S. Horike and A. Demessence, Cyclic Solid-State Multiple Phase Changes with Tuned Photoemission in a Gold Thiolate Coordination Polymer, *Angew. Chem., Int. Ed.*, 2022, **61**, e202117261.

14 Y. Hao, L. Yu, K. Miyazawa, S. Zhang, M. Liu, Z. Yu, J. Liu, Y. Yu, S. Li, S. Xu, T. Fukuma, S. X.-A. Zhang and M. Li, Highly Stable Triangular Single-Layer 2D Assemblies: Synthesis and Their Stimuli-Responsive Elastic and Anisotropic Curling, *Angew. Chem., Int. Ed.*, 2023, **62**, e202302365.

15 R. Bau, Crystal Structure of the Antiarthritic Drug Gold Thiomalate (Myochrysine): A Double-Helical Geometry in the Solid State, *J. Am. Chem. Soc.*, 1998, **120**, 9380–9381.

16 J.-U. Kim, S.-H. Cha, K. Shin, J. Y. Jho and J.-C. Lee, Synthesis of Gold Nanoparticles from Gold (I)–Alkanethiolate Complexes with Supramolecular Structures through Electron Beam Irradiation in TEM, *J. Am. Chem. Soc.*, 2005, **127**, 9962–9963.

17 H. Nie, M. Li, Y. Hao, X. Wang, S. Gao, B. Yang, M. Gu, L. Sun and S. X.-A. Zhang, Au(I)–thiolate nanostructures fabricated by chemical exfoliation and their transformation to gold nanoparticle assemblies, *J. Colloid Interface Sci.*, 2014, **434**, 104–112.

18 M. Liao, E. Cao, D. Julius and Y. Cheng, Structure of the TRPV1 ion channel determined by electron cryo-microscopy, *Nature*, 2013, **504**, 107–112.

19 Y. Li, Y. Li, A. Pei, K. Yan, Y. Sun, C.-L. Wu, L.-M. Joubert, R. Chin, A. L. Koh, Y. Yu, J. Perrino, B. Butz, S. Chu and Y. Cui, Atomic structure of sensitive battery materials and interfaces revealed by cryo-electron microscopy, *Science*, 2017, **358**, 506–510.

20 H. Nie, M. Li, Y. Hao, X. Wang and S. X.-A. Zhang, Time-resolved monitoring of dynamic self-assembly of Au(I)-thiolate coordination polymers, *Chem. Sci.*, 2013, **4**, 1852–1857.

21 H. Nie, M. Li, Y. Hao, X. Wang, S. Gao, P. Wang, B. Ju and S. X.-A. Zhang, Morphology modulation and application of Au(I)–thiolate nanostructures, *RSC Adv.*, 2014, **4**, 50521–50528.

22 C. Dai, Y. Hao, Y. Yu, M. Li and S. X.-A. Zhang, Kinetic Study on the Self-Assembly of Au(I)–Thiolate Lamellar Sheets: Preassembled Precursor vs Molecular Precursor, *J. Phys. Chem. A*, 2018, **122**, 5089–5097.

23 C. Dai, S. Xu, Y. Yu, M. Li and S. X.-A. Zhang, Unraveling Self-Carried Chemical Feedback on Assembly Processes and the Self-Termination of Growth in Au(I)–Thiolate Lamellae, *J. Phys. Chem. C*, 2020, **124**, 24400–24407.

24 S. Xu, S. Zhang, Y. Yu, S. Zhang and M. Li, Three-ligand Co-assembled 2D Au(I)-Thiolate Nanosheets, *Chem. – Eur. J.*, 2022, **28**, e202201968.

25 Bruker Axs., *Topas V5.0: General Profile and Structure Analysis Software for Powder Diffraction Data*, Bruker AXS Ltd, 2014.

26 M. J. Van Vleet, T. Weng, X. Li and J. R. Schmidt, In Situ, Time-Resolved, and Mechanistic Studies of Metal–Organic Framework Nucleation and Growth, *Chem. Rev.*, 2018, **118**, 3681–3721.

27 S. Popović, A. Tonejc and Ž. Skoko, Contemporary Diffraction Methods in Study of Polycrystals, *Croat. Chem. Acta*, 2015, **88**, 561–577.

28 A. Ponce, J. A. Aguilar, J. Tated and M. J. Yacaman, Advances in the electron diffraction characterization of atomic clusters and nanoparticles, *Nanoscale Adv.*, 2021, **3**, 311–325.

29 Y. Hao, C. Dai, L. Yu, S. Li, Y. Yu, B. Ju, M. Li and S. X.-A. Zhang, Solvent-induced stable pseudopolymorphism of Au(I)–thiolate lamellar assemblies: a model system for understanding the environment acclimation of biomacromolecules, *CrystEngComm*, 2018, **20**, 181–188.

30 S. Li, Y. Yu, J. Liu, S. Xu, S. Zhang, M. Li and S. X.-A. Zhang, Reactions Coupled Self- and Co-Assembly: A Highly Dynamic Process and the Resultant Spatially Inhomogeneous Structure, *Chem. - Asian J.*, 2019, **14**, 2155–2161.

31 O. Veselska, C. Dessal, S. Melizi, N. Guillou, D. Podbevšek, G. Ledoux, E. Elkaim, A. Fateeva and A. Demessence, New Lamellar Silver Thiolate Coordination Polymers with Tunable Photoluminescence Energies by Metal Substitution, *Inorg. Chem.*, 2019, **58**, 99–105.

32 C. Dai, Y. Yu, S. Xu, M. Li and S. X.-A. Zhang, Self-Templated Assembly of AuI/AgI-Thiolate Sheets with Central Holes, *Chem. - Asian J.*, 2019, **14**, 3149–3153.

33 X. Tang, W. Chen and L. Li, The Tough Journey of Polymer Crystallization: Battling with Chain Flexibility and Connectivity, *Macromolecules*, 2019, **52**, 3575–3591.

34 A. Elbanna, H. Jiang, Q. Fu, J.-F. Zhu, Y. Liu, M. Zhao, D. Liu, S. Lai, X. Chua, J. Pan, Z. Shen, L. Wu, Z. Liu, C.-W. Qiu and J. Teng, *ACS Nano*, 2023, **17**, 4134–4179.

35 C. Liu, L. Wang, J. Qi and K. Liu, Designed Growth of Large-Size 2D Single Crystals, *Adv. Mater.*, 2020, **32**, 2000046.

36 Y. Li, X. Jiang, Z. Fu, Q. Huang, G.-E. Wang, W.-H. Deng, C. Wang, Z. Li, W. Yin, B. Chen and G. Xu, Coordination assembly of 2D ordered organic metal chalcogenides with widely tunable electronic band gaps, *Nat. Commun.*, 2020, **11**, 261.